Hindawi
Advances in Materials Science and Engineering
Volume 2022, Article ID 7165240, 12 pages
https://doi.org/10.1155/2022/7165240

Research Article

Mechanistic Study of Rail Gouging during Hypersonic Rocket Sled Tests

Xuewen Zhou,[1,2] **Huadong Yan**,[2] **Cheng Chen**,[2] **and Yuanfeng Yu**[2]

[1]*School of Mechanical Engineering, Xi'an Jiaotong University, Xi'an 710049, China*
[2]*Test and Measuring Academy of Norinco Group, Huayin 714200, China*

Correspondence should be addressed to Huadong Yan; huadong_yan@163.com

Received 24 January 2022; Accepted 22 August 2022; Published 16 September 2022

Academic Editor: M. V. A. Raju Bahubalendruni

Gouging—an obstacle to the development of hypersonic rocket sled test techniques—was mechanistically investigated through experimental and theoretical analyses. Typical gouges were analyzed using macroscopic and microscopic experiments to investigate the evolution of gouging. Quasistatic compression and Hopkinson bar experiments were performed to systematically study the thermoviscoplastic properties of U71Mn rail steel under wide ranges of the strain rate and temperature. The critical condition for gouging was derived based on a thermoviscoplastic constitutive model supplemented by a three-variable criterion for an adiabatic shear instability. The results showed the following. (1) Adiabatic shear bands (ASBs) form when stress reduction under the combined action of frictional heating and high-speed deformation exceeds the strain-hardening effect of the rail material. (2) The nonuniform deformation of the edges of ASBs leads to the generation of cracks that split the rail surface. As the ASBs expand, the cracks grow and coalesce, eventually causing the material to peel off, forming gouges. (3) The relationships among the temperature, strain rate, and strain at the onset of gouging can be determined based on the critical condition for the formation of ASBs in rail steel.

1. Introduction

Rocket sled tests are a type of ground method for testing products during the whole ballistic process (including launch, flight, and impact) to evaluate whether factors such as their structural reliability and performance meet the design objectives. Specifically, in a rocket sled test, a product is examined in a simulated environment with the same Mach and Reynolds numbers as those in a real dynamic flight environment, where it is propelled by a rocket engine at a high velocity on a specifically constructed high-precision rail [1]. Figure 1(a) shows a photograph of a standby rocket sled waiting to be launched on a rail. Slippers are an important component of a sled that wraps around the rail head to enable rail travel at high velocities. To ensure smooth motion along a rail, a gap is left between the slippers and the rail, as shown in Figure 1(b). As a result, the sled is not always in contact with the rail and can fly in a free state and impact the rail at a well-defined frequency.

When the traveling velocity of a rocket sled approaches the hypersonic velocity, "raindrop"- or "spindle"-shaped gouges sometimes appear on the surface of the rail in contact with the slippers of the sled. This phenomenon first began to garner attention during rocket sled tests conducted in the United States in 1968 and was subsequently referred to as gouging [3, 4]. The occurrence of gouging sharply deteriorates the mechanical environment and, in severe cases, can even lead to rail fracture and the failure of a rocket sled test. Therefore, gouging significantly impedes velocity increases in rocket sled tests and has become a key issue facing the development of hypersonic rocket sled techniques that must urgently be addressed [5–7].

Through a metallographic examination of the gouges formed on a rocket sled rail made of AISI 1080 steel, Gerstle found that gouging is a thermomechanical event with sharp temperature changes accompanied by a phase change in the rail material [8]. Barber and Bauer found that when the traveling velocity of a sled reaches a certain value, the stress

(a) (b)

Figure 1: Rocket sled test system [2]. (a) A rocket sled waiting to be launched. (b) Mode of connection between a slipper and a rail.

formed from the impact of its slippers on the rail exceeds the limit strength of the rail material, thereby inducing gouging [9]. They defined the critical velocity at the onset of gouging as the "gouging threshold velocity." Mixon statistically analyzed data (e.g., sled velocities at the onset of gouging as well as the locations, quantities, and sizes of gouges) obtained from different rocket sled tests and, on this basis, inferred that the traveling velocity of the rocket sled, rail surface roughness, frictional heat, and impact force are the principal factors that induce gouging [10]. Using numerical analysis methods, Tachau et al. studied gouging in rocket sled rails, analyzed the causes and development of gouging, and put forward methods to mitigate gouging from material and structural perspectives [5, 6, 11–13].

The formation of adiabatic shear bands (ASBs) is considered one of the most important failure mechanisms of materials under impact loading [14–16]. An ASB typically forms under the action of a very large shear strain (10^0–10^2), which occurs in an almost flat narrow region (10^0–$10^2\mu m$) of the material over a very short time (10^0–$10^2\mu s$) and is accompanied by severe local temperature rises (that can be as high as 10^3 K) [17, 18]. Several scholars have studied the ASB from the perspective of continuum mechanics and proposed different adiabatic shear instability criteria. In the mid-1950s, Zener attributed the formation of ASBs to a thermoplastic instability that occurs locally in a material when the thermal softening effect exceeds strain- and strain-rate-hardening effects [19]. This concept quickly became a criterion for the initiation of adiabatic shear. In 1964, Recht noted that a local adiabatic shear instability occurs when the strain rate exceeds a critical value, which was used to establish a critical strain-rate criterion for adiabatic shear [20]. In 1973, Culver established a critical strain criterion [21]. However, both the strain rate and strain criteria are single-variable criteria that fail to comprehensively account for the effects of the temperature, strain, and strain rate on the critical condition for adiabatic shear. In 1987, Xu noted that the critical condition for adiabatic shear at a given ambient temperature depends on both the strain and strain rate [22]. Xu also studied the thermoviscoplastic properties and adiabatic shear deformation of a titanium alloy at high strain rates and correspondingly established a two-variable criterion that includes two critical control quantities, namely, the strain and strain rate. On this basis, in 1989, Bao incorporated the variation in the ambient temperature to derive a three-variable criterion that depends simultaneously on the strain, strain rate, and ambient temperature. The use of this criterion produced theoretical predictions in good agreement with experimental results [23].

An in-depth analysis of the conditions under which gouging occurs in a hypersonic rocket sled test was performed in this study: instead of only performing a phenomenological analysis and numerical simulation, gouges found on a rail made of U71Mn steel after a hypersonic rocket sled test were analyzed using macroscopic and microscopic methods to determine the evolution process for gouging. Then, quasistatic compression and Hopkinson bar experiments were performed to systematically investigate the dynamic mechanical properties of U71Mn rail steel over wide ranges of strain rates ($0.0005\,s^{-1}$–$8000\,s^{-1}$) and temperatures (25°C–800°C). On this basis, a thermoviscoplastic constitutive model was established and subsequently used in combination with a three-variable criterion for adiabatic shear instability to derive the critical condition for the occurrence of gouging in a U71Mn rail. It is hoped that the results of this study can provide a theoretical basis for future investigations on methods to mitigate gouging and, thereby, to promote the development of hypersonic rocket sled test techniques.

2. Macroscopic and Microscopic Analysis of Gouges

A hypersonic rocket sled test was conducted on a U71Mn rail. The slippers of the sled were produced using 30CrMnSiNi2A steel. Gouging occurred when the traveling velocity of the sled reached 1740 m/s. After the test, multiple gouges were discovered on the rail. These gouges were subsequently analyzed from macroscopic and microscopic perspectives to shed light on the initiation and evolution of gouging. Table 1 summarizes the chemical composition of U71Mn rail steel. The average hardness of the rail was 291 Brinell hardness (HBW).

2.1. Macroscopic Analysis of the Gouges. Figure 2 shows the morphology of two typical gouges. The gouges in Figures 2(a) and 2(b) are referred to as Gouges 1 and 2,

Table 1: Chemical composition of U71Mn rail steel (wt. %).

	C	Si	Mn	P	S
Measured	0.726	0.231	1.296	0.018	0.005
YB/T 5055-2014	0.65~0.76	0.15~0.58	0.70~1.40	≤0.035	≤0.030

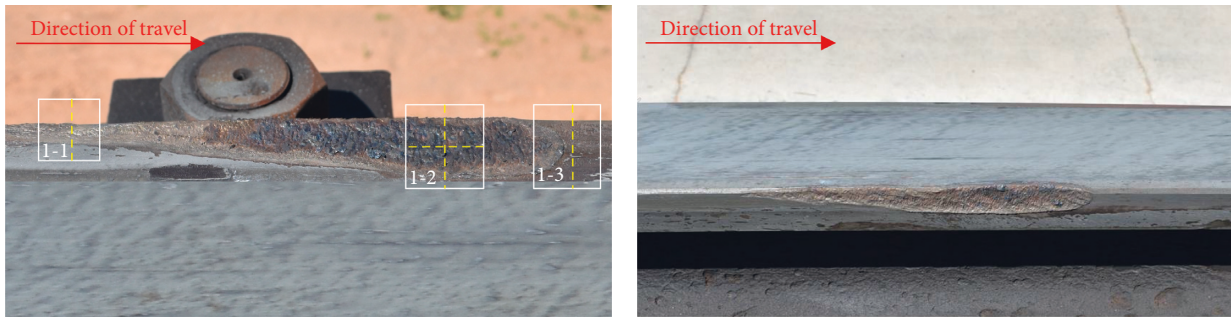

(a) (b)

Figure 2: Morphology of typical gouges. (a) A gouge formed at the top rail surface. (b) A gouge formed at an edge of the rail.

respectively. Gouge 1 formed on the top surface of the rail, and Gouge 2 formed at the junction of the top and lateral surfaces of the rail. The dimensions of the two gouges were approximately 150 mm × 26 mm × 1.5 mm and 196 mm × 13.5 mm × 1.8 mm.

These two gouges displayed a similar "raindrop" shape. Gouging occurred at the sharp tip and ended at the arc tail. Clear scratches were visible at the starting point of each gouge. The surface of each gouge was uneven and contained traces of the melted metal. The arc-shaped tail of each gouge rolled up because of an accumulation of melts. A macroscopic analysis revealed that the gouges were induced by the impact of the slippers on the steel rail during high-velocity flight and that the evolution of gouging was accompanied by a sharp increase in the temperature.

2.2. Microscopic Analysis of the Gouges. The initiation of gouging involves high-velocity, high-pressure, and high-temperature complex actions. Consequently, it is difficult to find suitable mechanical parameters to describe this phenomenon. Therefore, studying the microstructure surrounding the gouges has become an important means to investigate the evolution process of gouging.

Three samples (denoted as Samples 1–1, 1–2, and 1–3) were prepared from Gouge 1 to analyze the metallographic structure. Figure 2(a) shows the sampling sites. Samples 1–1, 1–2, and 1–3 were taken from the starting location of the gouge, the widest part of the gouge, and the location where the friction between the slipper and the rail continued after gouging stopped, respectively. Sample 1–2 was first subjected to a transverse metallographic examination, after which it was transected and then subjected to a longitudinal metallographic observation (the transverse and longitudinal directions refer to the directions perpendicular and parallel to the traveling direction of the sled, respectively).

An analysis of Figure 3 shows that a bright white structural layer (BWSL) formed on the metallographic surfaces of Samples 1–1, 1–2, and 1–3. However, the BWSL on the surfaces of Samples 1–1 and 1–3 was thinner than that on the surface of Sample 1-2. In addition, the pearlite and ferrite underneath the BWSL in Samples 1–1 and 1–3 did not undergo notable plastic deformation, whereas a 338.55 μm-thick plastic deformation layer formed beneath the BWSL in Sample 1-2.

3. Investigation of the Thermoviscoplastic Properties of U71Mn Rail Steel

Gouging is a complex process of material failure that depends on factors such as high temperatures and high strain rates. The flow stress response of U71Mn rail steel is highly sensitive to temperature and strain rate. Therefore, thermoviscoplastic analysis of U71Mn rail steel is a prerequisite for studying gouging in U71Mn rails [24]. Owing to its simple form and clearly defined parameters, the Johnson-Cook constitutive model is often used to describe the thermoviscoplastic behavior of materials [25–27]. Quasistatic compression and Hopkinson bar experiments were performed to determine the mechanical properties of U71Mn rail steel. Quasistatic compression experiments at room temperature were carried out according to standard GB/T 7314-2017, and Hopkinson bar experiments at room temperature were carried out according to standard GB/T 34108-2017. At present, there are neither high-temperature quasistatic compression experiment standards nor high-temperature Hopkinson bar experiment standards. Since the quasistatic compression experiment at room temperature and the high-temperature quasistatic compression experiment are very similar, this paper still refers to standard GB/T 7314-2017 when carrying out the high-temperature quasistatic compression experiment. The high-temperature

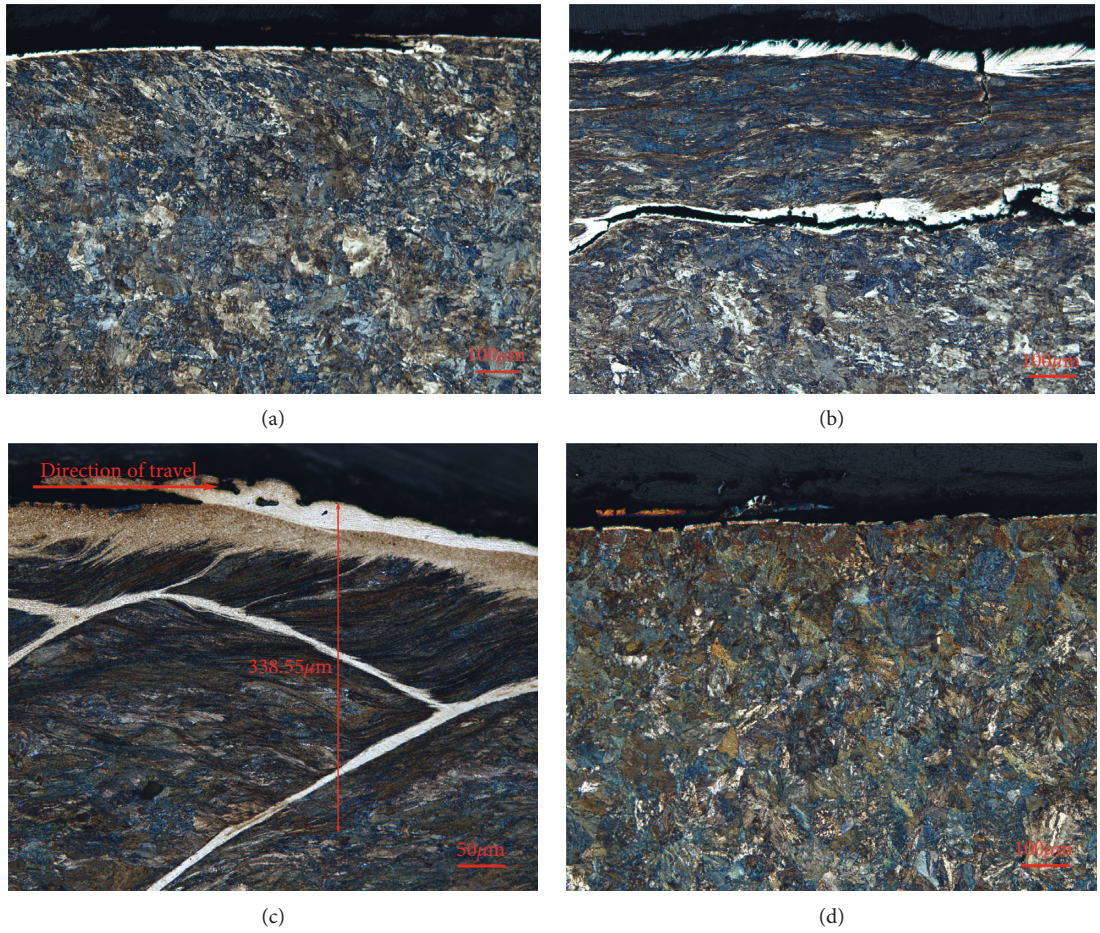

Figure 3: Metallographic structure of Samples 1–1, 1–2, and 1–3. (a) Sample 1–1. (b) Transverse ground surface of Samples 1–2. (c) Longitudinal ground surface of Samples 1–2. (d) Samples 1–3.

Hopkinson bar experiment involves synchronically assembled technology. When carrying out the high-temperature Hopkinson bar experiment, the experimental technology described in the literature [28] was referred to. On this basis, a Johnson-Cook constitutive model for U71Mn rail steel was established.

An LVF 100-1000 HH electrohydraulic servo universal material testing machine was used to perform quasistatic compression experiments on U71Mn rail steel at various strain rates ($0.0005\,s^{-1}$, $0.01\,s^{-1}$, and $0.1\,s^{-1}$) and temperatures (25°C, 200°C, 400°C, 600°C, and 800°C). The testing machine was capable of providing a load of ±100 kN and was equipped with an actuator with a stroke of ±75 mm. Cylindrical test samples with a size of ∅5 mm × 5 mm were prepared. The displacement–loading mode was used.

U71Mn rail steel was subjected to dynamic compression experiments on a split Hopkinson bar system at high strain rates ($800\,s^{-1}$, $3000\,s^{-1}$, and $10000\,s^{-1}$) and temperatures (25°C, 200°C, 400°C, 600°C, and 800°C). Experiments were conducted on three samples for each set of conditions. Cylindrical test samples with dimensions of ∅5 mm × 5 mm were prepared at $800\,s^{-1}$ and $3000\,s^{-1}$ strain rates, and cylindrical test samples with dimensions of ∅2 mm × 2 mm were prepared at a $10000\,s^{-1}$ strain rate. Under different strain rate conditions, different dimensions were produced for the incident, transmission, and impact bars used in the split Hopkinson bar system. The specific dimensions are shown in Table 2.

Within one-dimensional elastic wave propagation theory, the strain rate $\dot{\varepsilon}(t)$, strain $\varepsilon(t)$ and stress $\sigma(t)$ of a sample can be expressed as follows:

$$\dot{\varepsilon}(t) = -\frac{2C_0}{l_s}\varepsilon_R,$$

$$\varepsilon(t) = -\frac{2C_0}{l_s}\int_0^t \varepsilon_R \mathrm{d}t, \tag{1}$$

$$\sigma(t) = \frac{A_0}{A_s}E\varepsilon_T,$$

where A_0 is the cross-sectional area of the bar, E is the elastic modulus of the bar, $C_0 = \sqrt{E/\rho}$ (where ρ is the density of the compression bar) is the velocity of elastic longitudinal waves in the bar, A_s is the initial cross-sectional area of the sample,

Table 2: Specifications for split Hopkinson bar system device.

Strain rate (s^{-1})	Incident bar		Transmission bar		Impact bar	
	Diameter (mm)	Length (mm)	Diameter (mm)	Length (mm)	Diameter (mm)	Length (mm)
800	19	1200	19	1100	15	250
3000	19	1200	19	1100	19	150
10,000	5	400	5	400	5	80

l_s is the initial length of the sample, and ε_T and ε_R are the strains due to the transmitted and reflected waves at the end of the sample, respectively.

3.1. Effects of the Strain Rate on the Flow Stress. Figure 4 shows the true stress-strain curves of U71Mn rail steel at the experimental temperatures of 25°C, 200°C, 400°C, 600°C, and 800°C and different strain rates. Figure 5 shows the effects of the strain rate on the flow stress of U71Mn rail steel at $\varepsilon = 0.1$. The determined impact of the strain rates on flow stress is approximated at other strain values. Figure 4 shows that when U71Mn rail steel is subjected to quasistatic compression, the flow response of the material is only sensitive to the strain rate at the experimental temperatures of 600°C and 800°C. When U71Mn rail steel is subjected to dynamic compression, the specimen deforms but is not damaged. Therefore, the drop in the stress-strain curves corresponding to the 800 s^{-1}, 3000 $s^{-1,}$ and 10000 s^{-1} strain rates indicates unloading and not fracture. At the experimental temperatures of 25°C, 600°C, and 800°C, the flow stress approximately increases with the strain rate. However, at experimental temperatures of 200°C and 400°C, the flow stress at a strain rate of 10000 s^{-1} is less than the flow stress at a strain rate of 3000 s^{-1}.

Sample 1–1 was taken from the starting point of the sharp tip of the gouge, where slight gouging occurred. Sample 1–3 were taken from an area where no gouging occurred but where notable traces of friction were visible. Therefore, compared to Sample 1–2, which was taken from a severely gouged area, Samples 1–1 and 1–3 were only mildly impacted by the slipper. From this analysis, it can be inferred that the impact or frictional action of the slipper on the rail was the cause of the formation of a BWSL and that the thickness of the BWSL was related to the intensity of the interaction between the slipper and the rail.

When a slipper slides at a high velocity on or violently impacts a steel rail in a cold state, the heat generated from the sliding friction or impact causes a sharp increase in the local surface temperature of the steel rail, which in turn causes the pearlite to transform into austenite. However, as a result of the rapid heat transfer through the steel rail itself, the austenitized structure is quenched and therefore transforms into a martensitic structure. High hardness is a main characteristic of martensitic structures. To more accurately determine whether the BWSLs on the surface were martensitic in nature, a micro-Vickers hardness tester was used to measure the hardness of the bright white surface structures and matrix structures. The average hardness values for the bright white surface structures and matrix structures were found to be 805 and 286 HV0.3, respectively. Based on these hardness measurements, the bright white surface structures can be further determined to be martensitic.

ASBs at an angle of approximately 45° to the direction opposite to the traveling direction of the sled can be observed in the metallographic image of the longitudinal ground surface of Sample 1–2 (Figure 3(c)). These ASBs were phase-change shear bands with a width that tended to be uniform and undisturbed. The morphology of the original structure could no longer be distinguished at the center of the ASBs. In addition, elongated pearlite and ferrite grains surround the ASBs, whereas both the strain rate and the increase in the temperature were very high. As the matrix surrounding the ASBs underwent a small deformation and had a low temperature, the edges of the ASBs underwent uncoordinated deformation and were highly susceptible to microcracking, as shown in the metallographic image of the transverse ground surface of Sample 1–2 in Figure 3(b). The cracks divided the surface of the rail and propagated and grew as the ASBs extended, eventually causing the surface material to fall off continuously, creating gouges.

3.2. Effects of the Temperature on the Flow Stress. Figure 6 shows the true stress-strain curves of U71Mn rail steel at strain rates of 0.0005 s^{-1}, 0.01 s^{-1}, 0.1 s^{-1}, 800 s^{-1}, 3000 s^{-1}, and 10000 s^{-1} and different experimental temperatures. Specifically, as the experimental temperature increased, the flow stress decreased rapidly, i.e., U71Mn rail steel displayed strong thermal softening. However, at strain rates of 0.0005 s^{-1}, 0.01 s^{-1}, and 0.1 s^{-1}, the stress-strain curves of U71Mn rail steel at 400°C did not decrease as expected. Instead, a large part of or the entire stress-strain curves exceeded the stress-strain curves at 25°C and 200°C. This phenomenon resulted from a third type of strain aging of the material. To intuitively analyze the third type of strain aging phenomenon, the stress-strain curves at different temperatures are converted into the curves of flow stress as a function of temperature, as shown in Figure 7. The flow stress peaks at strain rates of 0.0005 s^{-1}, 0.01 s^{-1}, and 0.1 s^{-1} all appear at 400°C. However, as the strain rate increases, the peak stress gradually decreases.

To study the causes of the third type of strain aging phenomenon of U71Mn rail steel at high temperature, the microstructure of the samples after the quasistatic compression experiment at a strain rate of 0.0005 s^{-1} was observed. The optical microstructure of U71Mn rail steel, shown in Figure 8, is mainly flaky pearlite and sorbite. Figure 8 indicates that with the increase in the experimental temperature, the pearlite is deformed, fractured and refined

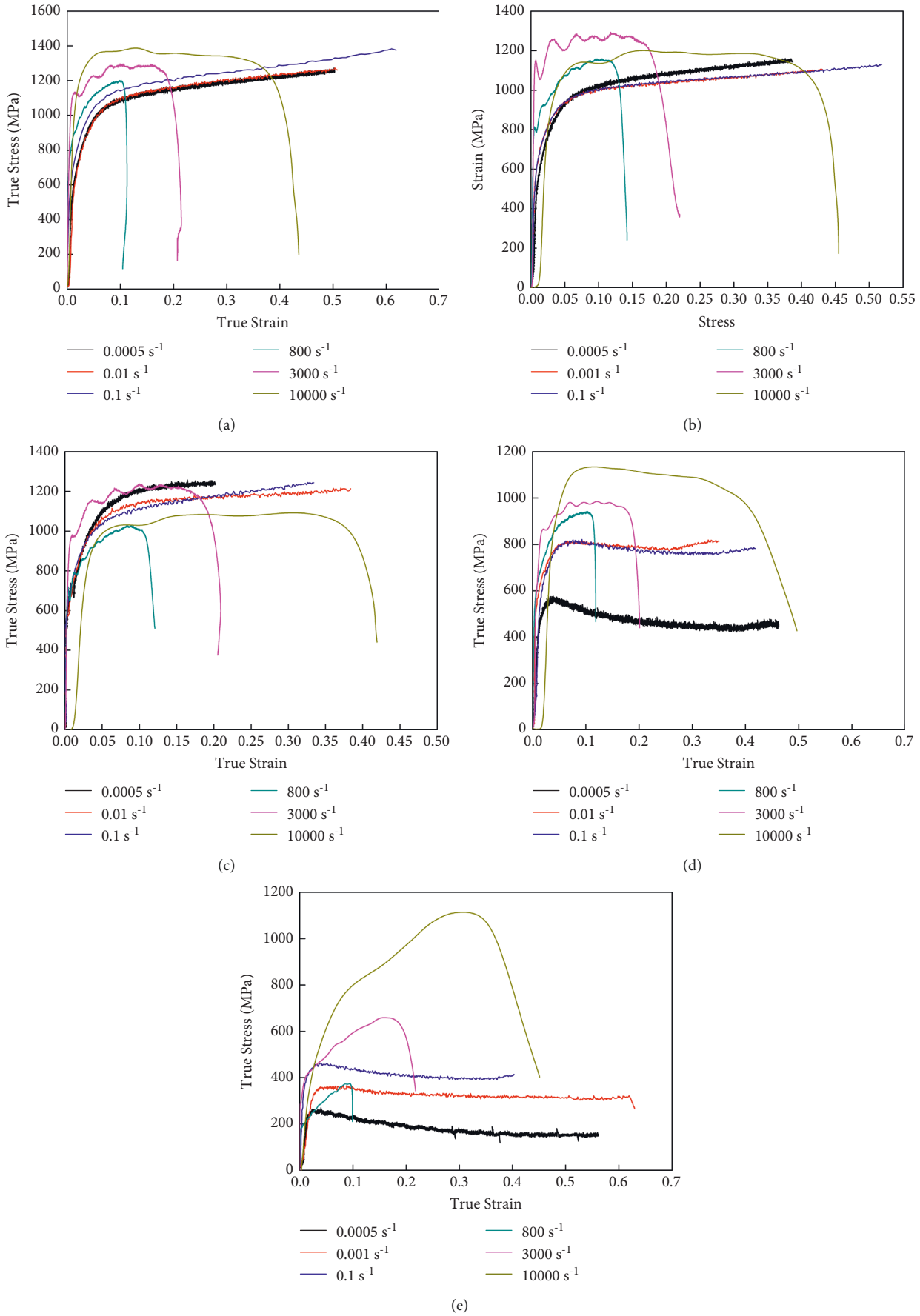

Figure 4: True stress-strain curves of U71Mn rail steel at different temperatures. (a) Experimental temperature: 25°C. (b) Experimental temperature: 200°C. (c) Experimental temperature: 400°C. (d) Experimental temperature: 600°C. (e) Experimental temperature: 800°C.

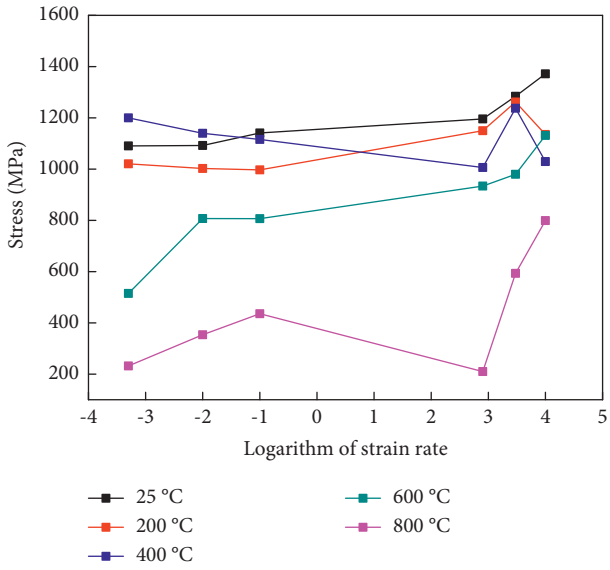

FIGURE 5: Effects of the strain rate on the flow stress of U71Mn rail steel at $\varepsilon = 0.1$.

after the sample is compressed; its lamellar spacing gradually becomes smaller, and it gradually becomes a fibrous structure. When the experimental temperature reached 400°C, the flaky pearlite was broken and dissolved into the matrix in a granular form, which enhanced the strength of the matrix and hindered the dislocation movement of the U71Mn rail steel. Therefore, in a certain temperature range, the flow stress of U71Mn rail steel does not decrease but rather increases with the increase in temperature.

3.3. Development of a Johnson-Cook Constitutive Model. The Johnson-Cook constitutive equation is an empirical model that accounts for the effects of the strain rate, strain, and temperature on the plastic flow stress and is given as follows:

$$\tau = \left(A + B\gamma^{n}\right)\left(1 + C\ln\dot{\gamma}^{*}\right)\left(1 - T^{*m}\right), \tag{2}$$

where γ is the equivalent plastic strain; $\dot{\gamma}^{*} = \dot{\gamma}/\dot{\gamma}_0$ ($\dot{\gamma}$ is the equivalent plastic strain rate, and $\dot{\gamma}_0$ is the reference strain rate and is set to 1 in this study); $T^{*} = (T - T_r)/(T_m - T_r)$ (T is the current temperature, T_r is the reference temperature and is set to room temperature, i.e., 25°C in this study, and T_m is the melting point of the material and is set to 1469°C in this study); A is the initial yield stress; B and n are parameters used to account for the strain-hardening effect; C is a parameter used to account for the strain-rate effect; and m is a parameter used to account for the temperature-softening effect.

First, the parameters in the first term (i.e., A, B, and n) of the Johnson-Cook constitutive model are determined by fitting the true stress–strain curve of U71Mn rail steel at a temperature of 25°C and a strain rate of 0.0005 s^{-1} obtained from the quasistatic compression experiments (Figure 5):

$$\tau = A + B\gamma^{n} - NY, USAes:\ (d). \tag{3}$$

Setting T to 25°C (i.e., $T = T_r$) simplifies the Johnson-Cook constitutive model to.

$$\tau = \left(A + B\gamma^{n}\right)\left(1 + Cln\dot{\gamma}^{*}\right). \tag{4}$$

The parameter C is determined by fitting the true stress-strain curves of U71Mn rail steel at an experimental temperature of 25°C and different strain rates.

Once the parameters A, B, n, and C have been determined, the parameter m can be expressed as follows:

$$m = \frac{\ln\left[1 - \tau/\left(A + B\gamma^{n}\right)\left(1 + Cln\dot{\gamma}^{*}\right)\right]}{\ln T^{*}}. \tag{5}$$

The parameter m can then be determined by fitting the true stress-strain curves of U71Mn rail steel at a constant strain rate and different temperatures.

The above fitting procedure was employed to yield a preliminary value for each parameter in the Johnson-Cook constitutive model for U71Mn rail steel. On this basis, the method of least squares was used to further optimize the values of the parameters of the model. Table 3 summarizes the final values of the parameters in the Johnson-Cook constitutive model for U71Mn rail steel.

4. Analysis of the Critical Condition for the Initiation of Gouging

Macroscopic and microscopic analyses showed that the gouges that occurred during the hypersonic rocket sled tests were caused by the adiabatic shear instability. Therefore, studying the adiabatic shear instability criteria for rail steels is very important for understanding the initiation and evolution of gouging.

Assuming that the shear stress τ of a material is a general function of the shear strain γ, strain rate $\dot{\gamma}$, and temperature T, the critical condition for adiabatic shear can be expressed as follows:

$$\frac{d\tau}{d\gamma} = \frac{\partial\tau}{\partial\gamma} + \frac{\partial\tau}{\partial\dot{\gamma}}\frac{d\dot{\gamma}}{d\gamma} + \frac{\partial\tau}{\partial T}\frac{dT}{d\gamma}. \tag{6}$$

The plastic work W done by external forces during the deformation of a material is expressed as follows:

$$W = \int_0^{\gamma} \tau\, d\gamma. \tag{7}$$

Under high-velocity impact, the heat generated in a material due to plastic deformation is unable to diffuse rapidly to the surrounding environment within a short period of time, resulting in an increase in the local temperature of the material. Denoting the plastic work-to-heat conversion coefficient by η yields.

$$\eta W \approx Q. \tag{8}$$

where Q is the heat generated when the material undergoes plastic deformation.

Plastic work is related to the adiabatic temperature increase at a high strain rate through the following equation:

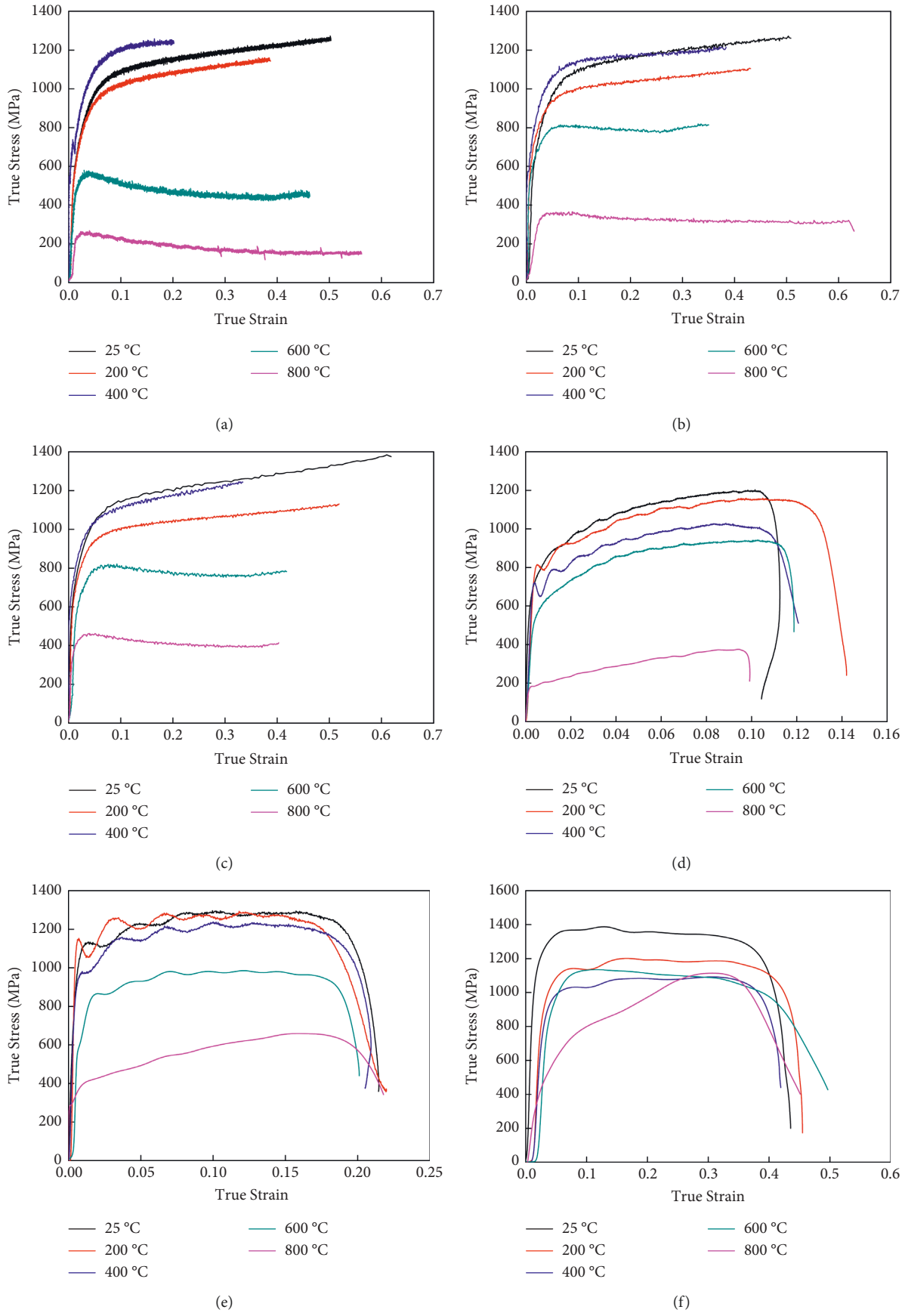

Figure 6: True stress-strain curves of U71Mn rail steel for different strain rates. (a) Strain rate: 0.0005 s^{-1}. (b) Strain rate: 0.01 s^{-1}. (c) Strain rate: 0.1 s^{-1}. (d) Strain rate: 800 s^{-1}. (e) Strain rate: 3000 s^{-1}. (f) Strain rate: 10000 s^{-1}.

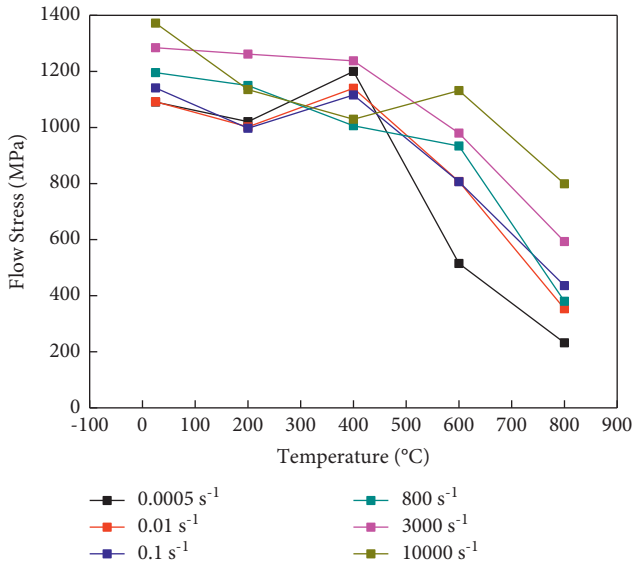

FIGURE 7: Effects of temperature on the flow stress of U71Mn rail steel at $\varepsilon = 0.1$.

$$\eta \int_0^{\gamma} \tau \, d\gamma = \rho C_v \Delta T, \tag{9}$$

where ρ and C_v are the density and constant-volume specific heat capacity of the material, respectively.

Then,

$$\Delta T = \frac{\eta}{\rho C_v} \int_0^{\gamma} \tau \, d\gamma. \tag{10}$$

Therefore, the adiabatic condition $dT/d\gamma$ can be expressed as follows:

$$\frac{dT}{d\gamma} = \frac{\eta \tau(\gamma, \dot{\gamma}, T)}{\rho C_v}. \tag{11}$$

The Johnson-Cook constitutive equation is used to derive the critical condition for adiabatic shear in U71Mn rail steel. $\partial\tau/\partial\gamma$, $\partial\tau/\partial\dot{\gamma}$, and $\partial\tau/\partial T$ are given below:

$$\frac{\partial \tau}{\partial \gamma} = nB\gamma^{n-1}\left(1 + C\ln\dot{\gamma}^*\right)\left(1 - T^{*m}\right), \tag{12}$$

$$\frac{\partial \tau}{\partial \dot{\gamma}} = \frac{C}{\dot{\gamma}}\left(A + B\gamma^n\right)\left(1 - T^{*m}\right), \tag{13}$$

$$\frac{\partial \tau}{\partial T} = -m\frac{T^{*m-1}}{T_m - T_r}\left(A + B\gamma^n\right)\left(1 + C\ln\dot{\gamma}^*\right). \tag{14}$$

During gouging, the strain rate depends collectively on the line-of-flight and vertical velocities of the sled when the slippers impact the rail. Relevant research shows that the vertical velocity of a sled does not exceed 3 m/s. Therefore, compared to the line-of-flight velocity, the effects of the vertical velocity on the strain rate are negligible. During a rocket sled test, the rocket engine is in operating mode and continuously provides a thrust throughout the slipper-rail interaction, and the impact of the slippers of the sled on the rail is an instantaneous process. Therefore, the line-of-flight velocity of the sled can be considered constant. In other words, the strain rate can be assumed to be constant. Then, $\partial\tau/\partial\dot{\gamma} = 0$. Therefore, equation (6) can be simplified to.

$$\frac{d\tau}{d\gamma} = \frac{\partial \tau}{\partial \gamma} + \frac{\partial \tau}{\partial T}\frac{dT}{d\gamma} = 0. \tag{15}$$

Substituting equations (11) and (12), (14) into equation (15) yields.

$$\left(1 + C\ln\dot{\gamma}^*\right)\left[nB\gamma^{n-1}\left(1 - T^{*m}\right) - \frac{m\eta\left(A + B\gamma^n\right)T^{*m-1}\tau(\gamma, \dot{\gamma}, T)}{\rho C_v\left(T_m - T_r\right)}\right] = 0. \tag{16}$$

The strain rate is greater than 1 during the slipper-rail interaction. Therefore, $1 + C\ln\dot{\gamma}^* > 0$. Then, equation (16) can be simplified to.

$$\frac{nB\gamma^{n-1}}{\left(A + B\gamma^n\right)^2} - \frac{m\eta\left(1 + C\ln\dot{\gamma}^*\right)\left(T - T_r\right)^{m-1}}{\rho C_v\left(T_m - T_r\right)} = 0. \tag{17}$$

Equation (17) is an algebraic equation with three variables, namely, the strain γ, strain rate $\dot{\gamma}$, and ambient temperature T, that represents a curved surface in a three-dimensional space with γ, $\dot{\gamma}$, and T as the coordinate axes. Substituting the values of ρ (7800 kg/m^3) and C_v (500 J/(kg·K)) of U71Mn rail steel, as well as η (1) corresponding to a high-velocity impact of slippers on U71Mn rails, into equation (18) yields the critical condition for gouging in U71Mn rails under impact by the slippers of a rocket sled during a hypersonic test, as shown in Figure 9.

Due to the considerable frictional and aerodynamic heat generated due to the slipper-rail interaction, there is an increase in the temperature of the slippers and the rail surface in local areas prior to gouging. According to Briggs, when a sled travels at a velocity of ≤6 Ma, the effects of aerodynamic heat in the slipper-rail gap are negligible relative to the frictional heat at the slipper-rail interface [29]. Therefore, based on the basic equation of heat transfer (equation (18)), the temperature increase due to slipper-rail friction can be numerically simulated to calculate the surface temperature of the rail at the onset of gouging:

$$\rho C_v \frac{\partial T}{\partial t} = \frac{\partial}{\partial x}\left(\lambda_x \frac{\partial T}{\partial x}\right) + \frac{\partial}{\partial y}\left(\lambda_y \frac{\partial T}{\partial y}\right) + \frac{\partial}{\partial z}\left(\lambda_z \frac{\partial T}{\partial z}\right) + \rho Q_T, \tag{18}$$

where Q_T is the intensity of the internal heat source in the object (unit: $W \bullet kg^{-1}$) and λ_x, λ_y, and λ_z are the heat transfer coefficients of the material along the x-, y-, and z-directions, respectively (unit: $W \cdot m^{-1} \cdot C^{-1}$).

Based on the boundary conditions for the hypersonic rocket sled test considered in this study, the increase in the surface temperature of the U71Mn rail due to frictional

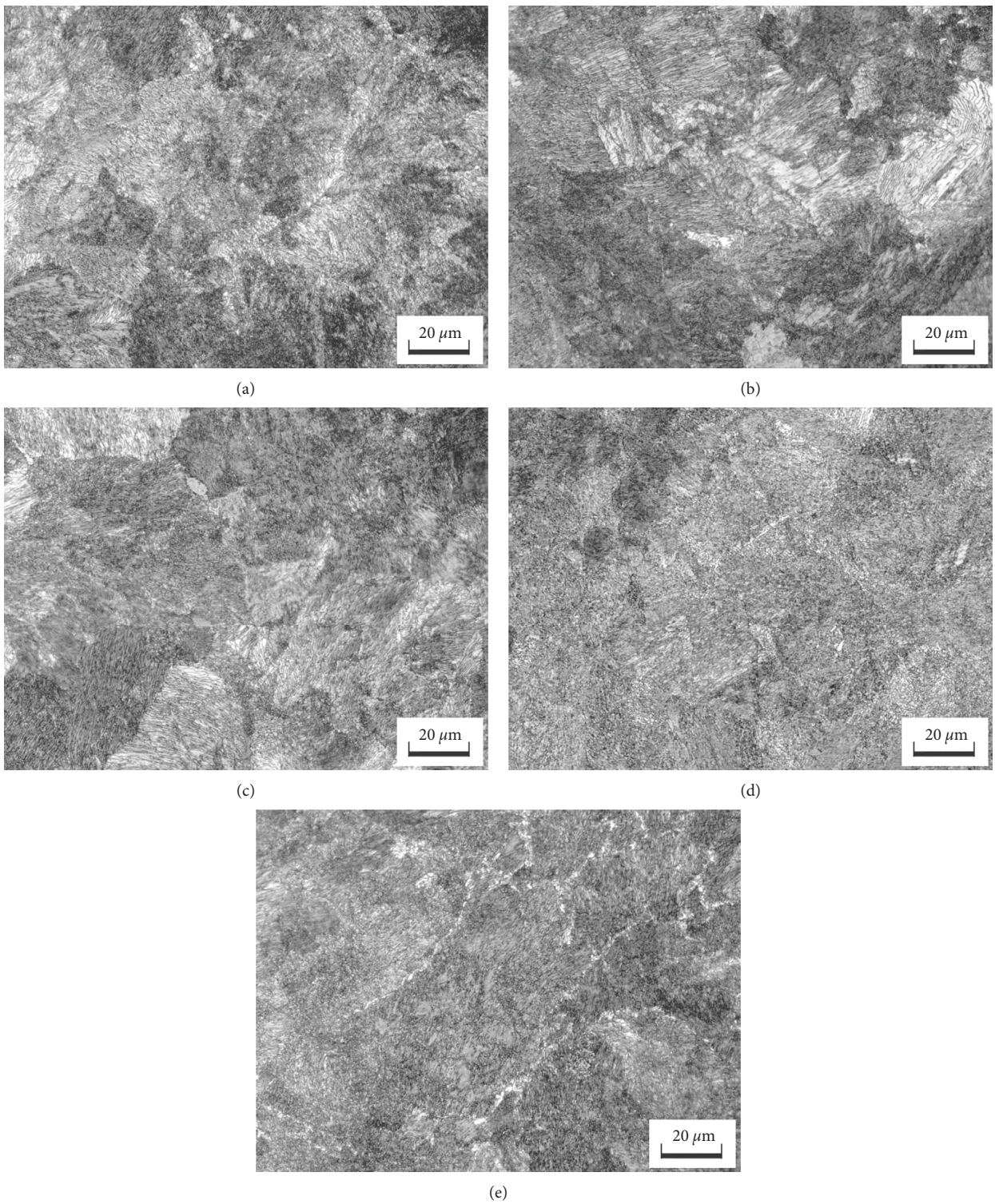

Figure 8: Microstructure of U71Mn rail steel at different experimental temperatures and a strain rate of $0.0005\,s^{-1}$. (a) Experimental temperature: 25°C. (b) Experimental temperature: 200°C. (c) Experimental temperature: 400°C (d) Experimental temperature: 600°C. (e) Experimental temperature: 800°C.

heat when the traveling velocity of the sled reached 1740 m/s (i.e., at the onset of gouging) was calculated. Under this condition, the surface temperature of the rail was found to be 560°C. The cumulative strain required for the initiation of gouging at a strain rate of $10000\,s^{-1}$ was found to be 0.388.

Table 3: Parameters of the Johnson-Cook constitutive model for U71Mn rail steel.

Parameter	A/MPa	B/MPa	n	C	m
Value	871	329.7	0.425	0.0186	1.26

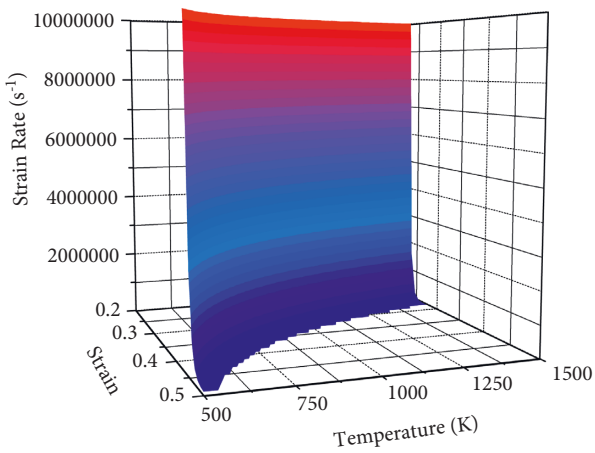

Figure 9: Critical condition for the initiation of gouging in a U71Mn steel rail.

5. Conclusion

In this study, the macroscopic and microscopic morphologies of the gouges on a U71Mn rail after a hypersonic rocket sled test were analyzed. Quasistatic compression and Hopkinson bar experiments were performed to study the thermoviscoplastic behavior of U71Mn rail steel. Based on a three-variable criterion for adiabatic shear instability, the critical condition for the initiation of gouging in U71Mn rails was derived. The following conclusions can be drawn from this study:

(1) The high-velocity impact of the slippers on the rail led to the formation of ASBs at an angle of approximately 45° with respect to the direction opposite to the traveling direction of the sled in the rail. The nonuniform deformation at the edges of these ASBs resulted in crack initiation. As the ASBs extended, the cracks propagated and grew, thereby separating the surface material of the rail into several pieces. Upon crack coalescence, the surface material of the rail fell off, eventually leading to the formation of gouges.

(2) The flow stress response of U71Mn rail steel is highly sensitive to the temperature and strain rate. The experimental results show that the strain rate had different effects on the flow stress of U71Mn rail steel at different temperatures, that is, the flow stress of U71Mn rail steel decreased rapidly as the experimental temperature increased.

(3) The increase in the temperature due to slipper-rail friction can be numerically simulated using the basic equation of heat transfer to calculate the rail surface temperature. Then, based on the critical condition for the formation of ASBs in U71Mn rails, the relationship between strain rate and strain at the onset of gouging can be determined.

Data Availability

The [DATA TYPE] data used to support the findings of this study are included within the article.

Conflicts of Interest

The authors declare that they have no known conflicts of financial interest or personal relationships that could have appeared to influence the work reported in this paper.

Acknowledgments

The authors would like to acknowledge the National Defense Science and Technology Innovation Special Zone Project of China (202011101).

References

[1] X. Zhou, J. Xu, and S. Lv, "Verification of a Verification of a ground-based method for simulating high-altitude, supersonic flight conditionsround-based method for simulating high-altitude, supersonic flight conditions," *International Journal of Computational Materials Science and Engineering*, vol. 7, no. 2, Article ID 1850005, 2018.

[2] J. S. Furlow, *Parametric Dynamic Load Prediction of a Narrow Gauge Rocket Sled*, Las Cruces: New Mexico State University, Las Cruces, New Mexico, 2006.

[3] K. F. Graff and B. B. Dettloff, "The gouging phenomenon between metal surfaces at very high sliding speeds," *Wear*, vol. 14, no. 2, pp. 87–97, 1969.

[4] J. D. Cinnamon, A. N. Palazotto, and A. G. Szmerekovsky, "Further refinement and validation of material models for hypervelocity gouging impacts," *AIAA Journal*, vol. 46, no. 2, pp. 317–327, 2008.

[5] R. D. M. Tachau, C. H. Yew, and T. G. Trucano, "Gouge initiation in high-velocity rocket sled testing," *International Journal of Impact Engineering*, vol. 17, no. 4-6, pp. 825–836, 1995.

[6] D. J. Laird and A. N. Palazotto, "Gouge development during hypervelocity sliding impact," *International Journal of Impact Engineering*, vol. 30, no. 2, pp. 205–223, 2004.

[7] C. D. Yeo, A. Palazotto, J. Song, and R Buentello, "Evaluation of thermomechanical damage of a slipper and rail in a rocket sled system," *Journal of Testing and Evaluation*, vol. 44, no. 4, Article ID 20140367, 2016.

[8] F. P. Gerstle, P. S. Follansbee, G. W. Pearsall, and M. Shepard, "Thermoplastic shear and fracture of steel during high-velocity sliding," *Wear*, vol. 24, no. 1, pp. 97–106, 1973.

[9] J. P. Barber and D. P. Bauer, "Contact phenomena at hypervelocities," *Wear*, vol. 78, no. 1-2, pp. 163–169, 1982.

[10] L. C. Mixon, "Assessment of Rocket Sled Slipper Wear/Gouging Phenomena," *Applied Research Associates, Inc., Rept.* F08635-97-C-0041 Albuquerque, NM, USA, pp. 33–47, 1997.

[11] D. J. Laird and A. N. Palazotto, "Effect of temperature on the process of hypervelocity gouging," *AIAA Journal*, vol. 41, no. 11, pp. 2251–2260, 2003.

[12] A. G. Szmerekovsky and A. N. Palazotto, "Structural dynamic considerations for a hydrocode analysis of hypervelocity test sled impacts," *AIAA Journal*, vol. 44, no. 6, pp. 1350–1359, 2006.

[13] A. G. Szmerekovsky, A. N. Palazotto, and W. P. Baker, "Scaling numerical models for hypervelocity test sled slipper-rail impacts," *International Journal of Impact Engineering*, vol. 32, no. 6, pp. 928–946, 2006.

[14] N. Yan, Z. Z. Li, Y. B. Xu, and M. A. Meyers, "Shear localization in metallic materials at high strain rates," *Progress in Materials Science*, vol. 119, Article ID 100755, 2021.

[15] Y. Z. Guo, Q. C. Ruan, S. X. Zhu et al., "Temperature rise associated with adiabatic shear band: causality clarified," *Physical Review Letters*, vol. 122, no. 1, Article ID 15503, 2019.

[16] Y. Z. Guo, Q. C. Ruan, S. X. Zhu et al., "Dynamic failure of titanium: temperature rise and adiabatic shear band formation," *Journal of the Mechanics and Physics of Solids*, vol. 135, Article ID 103811, 2020.

[17] S. M. Walley, "Shear localization: a historical overview," *Metallurgical and Materials Transactions A*, vol. 38, no. 11, pp. 2629–2654, 2007.

[18] D. Rittel, Z. G. Wang, and M. Merzer, "Adiabatic shear failure and dynamic stored energy of cold work," *Physical Review Letters*, vol. 96, no. 7, Article ID 75502, 2006.

[19] C. Zener and J. H. Hollomon, "Effect of strain rate upon plastic flow of steel," *Journal of Applied Physics*, vol. 15, no. 1, pp. 22–32, 1944.

[20] R. F. Recht, "Catastrophic thermoplastic shear," *Journal of Applied Mechanics*, vol. 31, no. 2, pp. 189–193, 1964.

[21] R. S. Culver, "Thermal instability strain in dynamic plastic deformation," *Metallurgical Effects at High Strain Rates*, pp. 519–530, Springer, New York, NY, USA, 1973.

[22] T. P. Xu, L. L. Wang, and W. X. Lu, "The thermoviscoplasticity and adiabatic shear deformation for a titanium alloy Ti-6Al-4V under high strain rates," *Explosion and Shock Waves*, vol. 7, no. 1, p. 18, 1987.

[23] H. S. Bao, L. L. Wang, and W. X. Lu, "The high velocity deformation and adiabatic shearing of a titanium alloy at low temperature," *Explosion and Shock Waves*, vol. 9, no. 2, pp. 109–119, 1989.

[24] J. Z. Pan, L. Chen, C. P. Liu, G. Zhang, and R Ren, "Relationship between the microstructural evolution and wear behavior of U71Mn rail steel," *Journal of Materials Engineering and Performance*, vol. 30, no. 2, pp. 1090–1098, 2021.

[25] T. Fourest, P. Bouda, L. C. Fletcher et al., "Image-based inertial impact test for characterisation of strain rate dependency of Ti6Al4V titanium alloy," *Experimental Mechanics*, vol. 60, no. 2, pp. 235–248, 2020.

[26] N. Selyutina, "Temperature relaxation model of plasticity for metals under dynamic loading," *Mechanics of Materials*, vol. 150, Article ID 103589, 2020.

[27] S. Liu, Q. Pan, H. Li et al., "Characterization of hot deformation behavior and constitutive modeling of Al–Mg–Si–Mn–Cr alloy," *Journal of Materials Science*, vol. 54, no. 5, pp. 4366–4383, 2019.

[28] Y. L. Li, Y. Z. Guo, H. T. Hu, and Q. Wei, "A critical assessment of high-temperature dynamic mechanical testing of metals," *International Journal of Impact Engineering*, vol. 36, no. 2, pp. 177–184, 2009.

[29] R. A. Briggs and R. H. Korkegi, "The hypersonic slipper bearing-a test track problem [J]," *Journal of Spacecraft and Rockets*, vol. 6, no. 2, pp. 210–212, 2012.